Dielectric Relaxation Studies of Acid-Containing Short-Side-Chain Perfluorosulfonate Ionomer Membranes

Z. D. Deng and K. A. Mauritz*

Department of Polymer Science, University of Southern Mississippi, Southern Station, Box 10076, Hattiesburg, Mississippi 39406-0076

Received August 26, 1991

ABSTRACT: The storage and loss components of the complex dielectric permittivities of aqueous H_2SO_4-containing short-side-chain perfluorosulfonic acid membranes were determined as a function of acid concentration and temperature. An equivalent circuit model and its mathematical representation is proposed for these ionomers. This simple, but successful, permittivity model reinforces our usual partitioning of the dielectric relaxation spectra into contributions that represent the short-range (intracluster) and long-range (intercluster) motions of ions throughout the known microphase-separated morphology. A low-frequency graphical feature on the experimental spectra that is reflective of and quantifies the tortuosity of long-range ion conductive pathways was identified and determined as a function of acid concentration and temperature. A high-frequency relaxation peak attributed to a fluctuating polarization that occurs at the cluster/TFE interfaces yields the time scales for intracluster ion motions and suggests the existence of two types of clusters for the case of low acid concentration.

Introduction

Perfluorinated ionomer membranes have been used, or suggested for use, in a number of industrial applications, such as ion-permselective separators in the electrochemical production of chlorine and caustic,[1,2] as well as in water electrolyzers, as battery separators,[3,4] as separators in fuel cells,[5] in photoelectrochemical systems,[6] and as strong acid catalysts for a number of reactions.[7] The earliest-reported perfluorosulfonate ionomer (PFSI) membranes were of the Nafion family and developed by E. I. du Pont de Nemours & Co. Dynamic aspects of ionic-hydration microstructures (i.e., side chain–counterion dissociation equilibrium, free vs bound water molecules, cation-mediated proton hopping within OH^--containing membranes), as well as main chain and polar cluster-related molecular motions in Nafion sulfonate materials in various counterion forms, have been studied extensively using infrared,[8-10] dynamic mechanical relaxation,[11-13] dielectric relaxation,[14-18] and solid-state multinuclear NMR[19-23] spectroscopies. Our IR and NMR studies of hydrated forms (for which the side chain to counterion mole ratio was 1:1) laid the groundwork for a theoretical model of membrane internal water activity and corresponding osmotic pressure.[23,24] Our IR studies of aqueous NaOH- and KOH-containing membranes provided deep molecular insight into the Na^+ and K^+ transport number vs caustic concentration dependence for membrane chlor-alkali electrochemical cells. Limited electron microscopic and extensive small-angle X-ray (SAXS) and small-angle neutron scattering (SANS) studies (as well as various inferential evidence from, for example, dielectric and mechanical relaxation studies) of long-range structure, in addition to wide-angle X-ray diffraction (WAXD) and differential scanning calorimetric (DSC) investigations of shorter-ranged structure, have led to the widely-accepted concept of a somewhat ill-defined hydrophilic/hydrophobic microphase separation in the form of sulfonate-rich ion clusters (~30–50 Å in diameter) embedded in a highly-crystalline[25] perfluorocarbon "matrix" wherein adjacent cluster "surfaces" are only on the order of a nanometer apart.[26-28] Gierke has suggested the existence of SO_3^--lined "pores" that connect adjacent clusters, but this concept has been criticized in a later literature review.[29]

More recently, Dow Chemical Co. has reported on the synthesis and characterization of a similar, but shorter-side-chained PFSI, whose structure, as compared to that of the long-side-chain (i.e., Du Pont) PFSI, is seen in Figure 1. It has been reported that this short-side-chain PFSI exhibits exceptional performance as a high-current-efficiency, low-power-consumptive separator in chlor-alkali cells.[30] Tant, Darst, Lee, and Martin[31] studied the structure and properties of the short-side-chain PFSI's as compared to the long-side-chain counterpart. Extensive and systematic dynamic mechanical relaxation, DSC, and WAXD studies were performed by these investigators on these materials in the sulfonyl fluoride, sulfonic acid, and sodium sulfonate forms. Amongst the wealth of information in their report, it is interesting to note that the short-side-chain materials can exhibit two types of crystallinity and, on a comparative basis, display higher Tg's than their long-side-chain counterparts, the T_g for the Na^+ form being higher than that of the acid form for the same equivalent weight (EW). We feel that this information will ultimately be important in establishing relationships between the microstructure and molecular motions within these polymers and the selective transport of hydrated ions through the microstructure. As with the Nafion materials, the short-side-chain PFSI's are considered to possess polar/nonpolar microphase separation as well as a TFE-like crystallinity, as first reported in the public literature by Moore and Martin, based on SAXS, WAXD, and DSC studies.[32]

In order to better understand relationships between important aspects of ionic transport (e.g., ion permselectivity, steady-state current power consumption) and the chemical structure and resultant morphology of the short-side-chain PFSI membranes, we have initiated an analysis of these systems using dielectric relaxation spectroscopy and the structure–(dielectric) property concept we have established based on our prior investigations of the long-side-chain PFSI's.

In recent reports by Mauritz et al.,[14-17] it was rationalized how the dielectric relaxation spectra of Nafion PFSI membranes, that were equilibrated in various aqueous electrolyte solutions, were diagnostic of long- and short-range motions of hydrated ions throughout the heterophase morphologies of these systems. The signature of the long-

0024-9297/92/2225-2369$03.00/0

(a) (b)

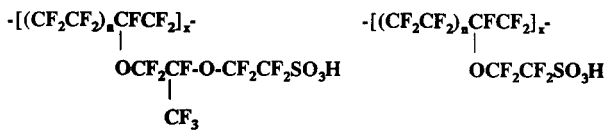

Figure 1. Chemical structures of the (a) long-side-chain (Nafion) and (b) short-side-chain (Dow Chemical Co.) perfluorosulfonate ionomers in the acid forms.

range motions (i.e., intercluster hopping) of ions consists of a linear segment in the low-frequency region of log ϵ'' vs log f plots, where ϵ'' is the dielectric loss factor and f is the frequency of the applied electric field. In effect, the loss spectra for all electrolyte-imbibed membranes can be curve-resolved into the following linear superposition:

$$\epsilon'' = \epsilon_{ac}'' + A\omega^{-n} \tag{1}$$

where $\omega = 2\pi f$, A is a (curve-fitted) constant, and n, the fitted slope of the linear segment of the curve, is considered to be a coarse morphological parameter in the following sense. We have, in our earlier works, labeled the last term in eq 1 as ϵ_{dc}''. It was reasoned in our earlier papers that, for a given PFSI, EW, as well as imbibed electrolyte concentration and counterion and co-ion type, and temperature, as well as, say, membrane pretreatment conditions, the experimentally-extracted parameter n is reflective of the overall *connectivity* of the macroscopic ensemble of ionic clusters. Considering the great width of the single SAXS peak displayed by these materials, it is quite easy to imagine that there must exist a broad distribution of ionic cluster sizes and intercluster spacings. In short, there is considerable disorder in the packing of clusters. Therefore, one might expect the energetic barriers for intercluster ion hopping to consequently have a significant distribution. Energetic barriers, in our view, involve the tortuous motions of ions around the cluster-intervening TFE microcrystallites, perhaps between disordered, less-tightly packed, TFE tie molecules. Effectively then, dead ends, or charge traps, exist over the ion-conductivity grid. Perhaps the geometry/topology and rate-limiting energetics of long-range ion hopping might best be viewed within the mathematical framework applied to processes that are *fractal* in space or time, or both. Crude theoretical, but basically non-structurally-specific, models of the "universal dielectric response of heterogeneous materials" might suggest that n should lie between 0 and 1,[17] with lower values of n representing lower degrees of structural disorder. $n = 1$ would correspond to pure ionic drift, while $n = 1/2$ indicates totally-random ionic pathways, i.e., diffusion. There is, however, no theoretical reason as to why n cannot exceed a value of 1, and the application of the dielectric relaxation analysis of these systems should not be prejudiced by the highly-undeveloped state of theory in this general area. The latter situation, that is $n > 1$, would reasonably indicate highly-interconnected ion-conduction pathways.

The ϵ_{ac}'' term in eq 1 is meant to represent the always-observed high-frequency *relaxation peaks* that are often obscured by the "dc effect". In practice, ϵ_{ac}'' vs ω curves are extracted by the point-by-point subtraction of fitted $A\omega^{-n}$ values from ϵ'' over the high-frequency range in accordance with eq 1. This relaxation has been attributed to the cluster-confined motions of hydrated mobile ions. In a number of cases, the temperature shift of the frequency corresponding to the peak maximum, ω(or f)$_{max}$, is Arrhenius-like, yielding a well-defined activation energy. The relaxation time, $\tau = \omega_{max}^{-1}$, is taken as the time scale

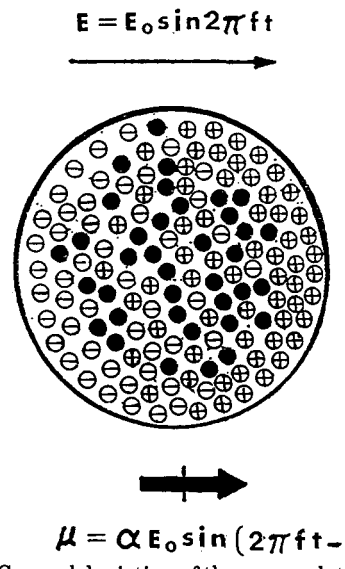

Figure 2. General depiction of the accumulation of ionic charge at the hydrophilic/hydrophobic phase boundaries, due to thermal fluctuation, resulting in an induced cluster dipole of moment μ. α is the cluster polarizability, and δ is the phase angle by which μ lags behind the oscillating applied electric field, **E**, due to resistance to intracluster migration.

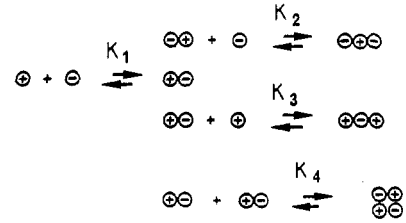

Figure 3. Schematic representation of the equilibrium between low-order ionic associations in cluster-contained electrolytes. The K_i's are hypothetical, temperature, and concentration-dependent equilibrium constants.

associated with the accumulation and dissipation of ionic charge at the hydrophilic/hydrophobic phase boundaries in cooperative fashion, as depicted in Figure 2. τ has been observed in our work to be quite sensitive to the concentration of imbibed electrolyte. This concentration sensitivity has been attributed to the progressive association of incorporated ions into electrically-neutral pairs, charged triplets, or motionally-sluggish, higher-order multipoles with increasing concentration, as depicted in Figure 3. We believe that this *relaxation of interfacial polarization* mainly arises because of the obvious gradients of the mobilities of the cations and anions across hydrophilic/hydrophobic interfaces in the direction of the applied electric field. It is believed that the enormous values of ϵ' at the lowest frequencies are due to this significant polarizability mechanism, as well. We further suggest that the width of this peak, in part, might result from a distribution of cluster sizes, which, in turn, might be due to a microscopic distribution of equivalent weight. The straightforward rationale behind this thought is that the magnitude of interfacial polarization of a given cluster should be proportional to its corresponding interfacial surface area. A distribution of cluster surface/volume ratios will therefore generate a distribution of relaxation times. While the above dielectric relaxation analysis and underlying mechanistic concepts have been reported exclusively for the long-side-chain PFSI membranes, a similar investigation can be useful in understanding the nature of long- and short-ranged ion motions and, ultimately, membrane structure/ion transport relationships

for the Dow short-side-chain PFSI membranes.

Experimental Section

PFSI membranes of 795, 964, and 1001 EW were formulated and supplied by Dow Chemical Co. through the efforts of C. W. Martin. All membranes, having a nominal thickness of ~0.18 mm, were systematically initialized using the standard procedure described below before performing the electrolyte uptake, followed by the dielectric relaxation experiments. The membranes were first equilibrated in 14 M H_2SO_4 solutions for 48 h to ensure the conversion, by ion exchange, of all of the fixed sulfonate groups to the desired acid form. Then, the films were soaked in deionized water for 48 h to extract the excess H_2SO_4 component. At this point, the samples are expected to contain no SO_4^{2-} anions, which have leached out into the pure water bath owing to H^+ and SO_4^{2-} diffusional gradients, but the membranes will be swollen with a considerable amount of water. Having been dried at 100 °C under vacuum for 48 h, the membranes were stored in a desiccator until the controlled uptake of H_2SO_4 was affected. This standard membrane initialization protocol was uniformly applied in order to ensure that all samples entered experimentation being in the same chemical state and having experienced the same swelling and thermal histories.

All the membranes, initialized in this way, were subsequently imparted various internal concentrations of H_2SO_4 as follows. The membranes were equilibrated in aqueous H_2SO_4 solutions of various concentrations (1–14 M) at constant temperatures (ranging from 22 to 65 °C) for at least 48 h. The high acid concentrations used were intended to generate the possibility of the earlier-discussed ion association effects. Donnan theory[33] prescribes the equilibrium distribution of the concentration of diffusible ions across a membrane/electrolyte interface, given the initial ion concentrations as well as the initial concentration of membrane-affixed charges. It is our opinion that this theory is not directly applicable to membranes (a) having fixed charges that are *clustered* and (b) that are equilibrated in highly concentrated solutions wherein the short-range ionic structures that are depicted in Figure 3 can form. In situation b, the required single ion activity coefficients within the membrane are unknown, thus preventing the use of the Donnan theory. We have commented on the major problems involved with the use of this simple theory within the context of clustered ionomers in earlier papers.[9,14] Furthermore, we have demonstrated, for the case of aqueous NaOH-containing Nafion sulfonate membranes, that an accounting for membrane swelling as well as for the clustering of ion-exchange groups (as opposed to an assumed homogeneous distribution) still does not bring the standard Donnan equilibrium theory in line with the actual internal vs external concentration profile as determined by careful membrane titration and mass uptake.

The membranes were removed from the acid solutions, surface-blotted dry, and immediately placed in a temperature-controlled, parallel-plate electrode test cell. Electrical impedance measurements were taken over the frequency range of 5–10 MHz using an HP 4192A low-frequency impedance analyzer controlled by a PC through a GPIB. The applied sinusoidal voltage signal had a root-mean-square amplitude of only 5 mV so that the electrical response can be expected to be linear, as desired. Also, the impedance data were corrected for the contribution from the empty cell. Impedance data were converted to the real, or storage (ϵ'), and imaginary, or loss (ϵ''), components of the complex dielectric permittivity, $\epsilon^* = \epsilon' - i\epsilon''$, at each tested frequency.

Theoretical Background

Electrical impedance, Z^*, was converted to the complex dielectric permittivity using the equation

$$\epsilon^* = l(i\omega\epsilon_0 A_c Z^*)^{-1} = \epsilon' - i\epsilon'' \qquad (2)$$

where ϵ_0 is the dielectric permittivity of free space (8.854×10^{-12} F/m), A_c is the electrode surface area, and l is the thickness of the membrane. In general terms, ϵ' is a measure of the degree of charge polarization, or the energy involved in affecting this separation of charge. ϵ'', on the other hand, is a direct measure of the energy that is irreversibly dissipated within the time frame of the relaxation of polarization. As in our previous studies of PFSI membranes, the familiar molecular dipole orientation mechanism of Debye is not considered to be as significant as either the interfacial polarization or the long-range ion-hopping mechanisms for these more complex systems.

As mentioned, the curve-resolved ϵ_{ac}'' vs ω peaks are believed to arise from highly polarizable, hydrated ionic clusters which in effect act as ca. 40-Å-in-size fluctuating macrodipoles. On the other hand, mobile ions will be capable of executing increasingly greater net displacements during a half-cycle of the applied voltage signal during which time the electric field is in the same direction, as the frequency decreases. The latter process, in short, is believed to give rise to the long-range transport term, ϵ_{dc}''.

A rather simple model of dielectric loss attributed to long-range ion transport (excluding short-range ion motions or molecular dipole reorientations) consists of a linear superposition of two familiar processes: (1) ionic drift under an applied *unidirectional* electric field; (2) random diffusion of mobile ions. On the basis of this simple concept in which the net ion transport is formally divided proportionately between these two well-defined kinematic mechanisms, we have derived the following equation for ϵ_{dc}'' for a single charge carrier under the influence of an applied *square* (rather than sine) wave of frequency f[34]

$$\epsilon_{dc}'' = K_1/f + K_2/f^{1/2} \qquad (3)$$

where K_1 and K_2 are frequency-independent constants that are, at the least, functions of the number density, electrical mobility, and diffusion coefficient of the charge carrier, as well as the amplitude of the applied electric field in the form of a square wave. In the interest of brevity, we omit the derivation of this equation, the numerous details of which will appear in a future paper. However, it should be mentioned that the use of a square, rather than sine, wave in the derivation not only renders the mathematical analysis considerably more simple, as well as simulate a closer-to-dc-like condition during an electrical half-cycle, but also the results in fact should be identical, as it has been established that *small* electrical amplitude techniques, as the one used in these studies, lead to the same impedance regardless of the specific excitation waveform.[35]

When $K_1 \gg f^{1/2}K_2$, the low-frequency linear segment on the log ϵ'' vs log f spectra will have a slope approaching −1, whereas if $K_1 \ll f^{1/2}K_2$, the slope will be close to −0.5. Of course, hybrid situations between the drift- and diffusion-dominant cases can be envisioned which would yield effective values of n that are neither 1 nor 0.5. This simple model, at least, provides an interpretive framework for dc-dominated dielectric loss spectra, such as those encountered throughout this work. An obvious shortcoming of this model is a lack of interpretation for experimentally-derived values of n that are less than 0.5. In this case, the fractal concept of ill-connected charge pathways would seem to be applicable.

The impedance response of a membrane can be modeled using an *equivalent circuit* assembled from resistive, capacitive, and diffusive elements. This practice in electrical theory has a mechanical analogy in the representation of the viscoelastic phenomena exhibited by polymers by springs and dashpots. Such models are also attractive in electrical impedance spectroscopy, since the frequency response of linear electrical circuits is well understood. Of course, incorporated circuit elements should represent some aspect of predominant molecular

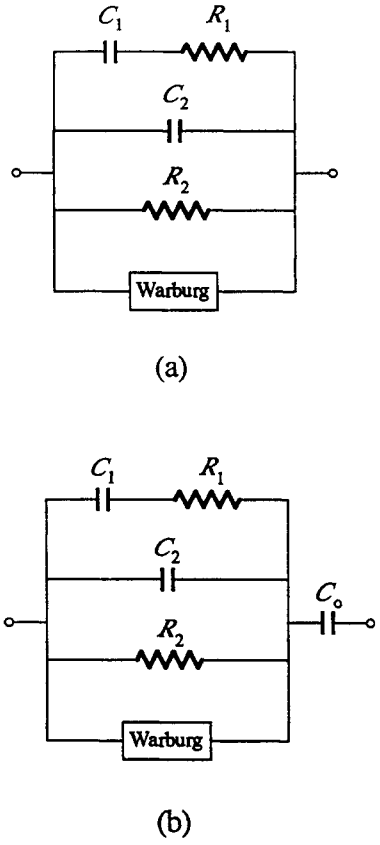

Figure 4. Equivalent impedance circuit for (a) an electrolyte-imbibed ionomer membrane with ionic clusters and (b) the same membrane but with membrane/electrode interfaces present.

processes. An equivalent circuit containing a minimal number of elements that we propose to be reasonable for a hydrated ionomer membrane containing mobile ions is shown in Figure 4a. The elements R_1, C_1, and C_2 compose a lumped "Debye" element that is intended to represent the single relaxation peak usually observed in our experimental ϵ_{ac}'' vs ω curves. These three lumped elements are meant to account for short-range (i.e., intracluster) ion motions, as the current-blocking capacitor C_1 will prevent long-range (electrode-to-electrode) charge transport through this electrical branch. C_1, in essence, accounts for the overall capacitance associated with the cumulative effect of individual cluster polarization, whereas R_1 accounts for the energy dissipated in affecting this polarization. Ionic migration, or drift, is represented by the pure resistor, R_2. Ionic diffusion (i.e., random, nondirected long-range ion motion) is represented by the complex Warburg impedance element, Z_w, that is commonly employed in the modeling of electrochemical systems. The equation for the Warburg impedance presented below actually refers to a single diffusing counterion, e.g., H^+, or more precisely H_3^+O, in a situation where there are no diffusing co-ions and the H^+ to SO_3^- mole ratio is 1:1.[36] The existence of co-ions (e.g., SO_4^{2-} anions) would slightly complicate the expression, but the dependence of Z_w on ω would remain the same:

$$Z_w = RT(zF)^{-2}(i\omega D)^{-1/2}C^{-1} \quad (4)$$

where R is the gas constant, T the absolute temperature, z the charge on the diffusing ion, F the Faraday constant, C the mobile ion concentration, and D the diffusion coefficient of the mobile ion. The complex permittivity for the equivalent circuit shown in Figure 4a can easily be

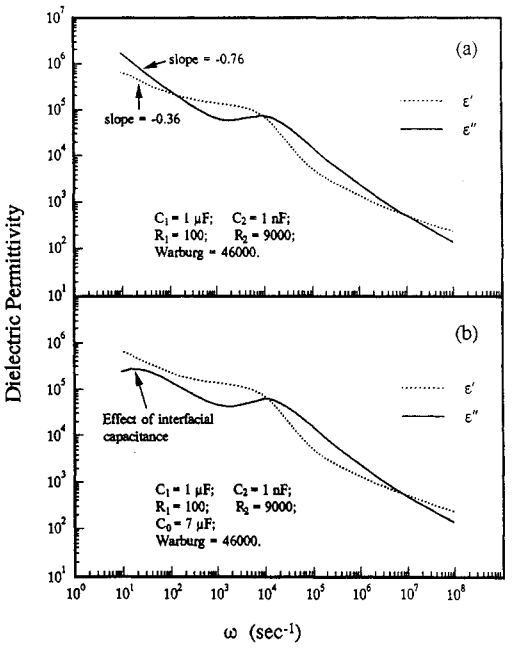

Figure 5. Theoretical dielectric relaxation storage and loss spectra corresponding to the equivalent circuits a and b in Figure 4, respectively. The listed circuit element values are hypothetical. The downturn in the loss spectrum seen at the lowest frequencies in b is due to membrane/electrode interfacial polarization.

derived and is given by the equation

$$\epsilon^* = \frac{C_2}{\epsilon_0} + \frac{C_1 - i\omega C_1^2 R_1}{[(\omega C_1 R_1)^2 + 1]\epsilon_0} - \frac{i}{R_2\omega\epsilon_0} - \frac{i-1}{2W\omega^{1/2}\epsilon_0} \quad (5)$$

where W is the frequency-independent Warburg constant given by $RT/[(zF)^2C(2D)^{1/2}]$.

Figure 5a shows hypothetical log–log plots of both the loss and storage dielectric permittivities as a function of ω as calculated from eq 5 using the indicated sample values of capacitance, resistance, and the Warburg constant. The log ϵ'' vs log ω plot does in fact display a linear segment at low frequencies with a slope between 0.5 and 1.0 and a noticeable relaxation peak at high frequencies that is due to the second term in eq 5 at $\omega = 10^4$ s^{-1} ($=1/(R_1C_1)$). The reverse S-shaped log ϵ' vs log ω plot also has a linear segment in the low-frequency regime with an apparent slope that is less than 0.5. The significant fact concerning these hypothetical plots is that, over the entire frequency range, the general relaxation behavior exhibited by the hydrated, ion-containing PFSI membranes, as obtained by experiment, appears to be well-modeled by this equivalent circuit representation.

The membrane/electrode interface is considered as "blocking" in that mobile ions cannot pass across it. This situation would theoretically call for a capacitance, C_0, to be placed in series with the totality of lumped elements representing the PFSI membrane, as shown in Figure 4b. The analytical equation for the equivalent circuit in Figure 4b is in fact too unwieldly to be of simple practical use. However, numerical results can again be generated by substituting appropriate values for all the circuit elements, and the results for a given sample set are shown in Figure 5b. On comparing parts a and b of Figure 5, it is apparent that this interfacial capacitance only affects ϵ'' at the lowest frequencies. ϵ'' values curve downward with decreasing frequency, illustrating the current-limiting effect of this capacitor. Other than this perturbation, the long- and short-range ion-transport-associated features are present on the curve, as before. However, in the mathematical

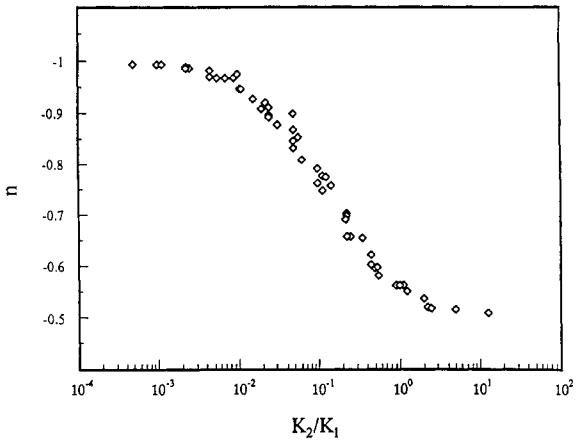

Figure 6. Effective slope of the low-frequency linear segment of theoretical log ϵ'' vs log f curves vs the ratio K_1/K_2 calculated using eqs 3 and 5.

analysis of our experimental results, this feature was ignored, as it is not strongly linked to the ion motions within the bulk of the membrane, which is our primary interest in these studies.

On comparing the coefficients of the ω^{-1} and $\omega^{-1/2}$ terms in eq 3 with the corresponding terms in the imaginary part of eq 5, it is seen that $K_1 = 1/(R_2\epsilon_0)$ and $K_2 = 1/(2\epsilon_0 W)$. Figure 6 shows an *effective* or hybrid n as calculated from eq 5, as a function of the ratio K_2/K_1. As expected, at low K_2/K_1, the migration (drift) process is dominant, n being close to 1, while at high K_2/K_1 the diffusion process is favored as n approaches 0.5. The scattering within the sampled data points is an artifice caused by the choice of a finite lower limit of the experimentally-attainable frequency (5 Hz). With reference to Figure 6, it is seen that the relative weight of diffusion vs drift control, as a function of n (an experimentally-derived quantity), is most sensitive to n at the extreme values of this parameter ($^1/_2$, 1) and is least sensitive at values close to the median value (0.75).

Results and Discussion

Having equilibrated the sulfonic acid membranes in aqueous H_2SO_4 solutions, the clusters are swollen with water molecules, H^+ "ions" (i.e., H_3O^+ species), and SO_4^{2-} anions. As the external electrolyte concentration increases, the clusters become less hydrated. Thermodynamically, as the water activity in the external solution becomes depressed, there is a diminished driving force for water to enter the membrane, although the internal ionic concentration will increase due to increased chemical potential gradients for the mobile ions.

There are a number of graphical features that are common to the dielectric relaxation spectra of all the tested membranes, regardless of acid bath concentration, temperature, or EW. These common features include (1) extremely high low-frequency-limit dielectric constants, ϵ_0' and ϵ_0'' (on the order of 10^6–10^7), (2) largely monotonically decreasing (save for superimposed high-frequency peaks) ϵ' and ϵ'' vs f behavior, (3) distinct linear segments in the low-frequency regions on the loss spectra, and (4) relaxation loss peaks that can be resolved in the high-frequency domain.

As in our similar dielectric relaxation studies of the long-side-chain PFSI's, we attribute situation 1 to an extreme polarizability associated with the hydrated, ion-containing clusters. In short, hydrophilic/hydrophobic interfacial polarization has a longer time to develop with lower frequency; this gives rise to a large induced dipole moment

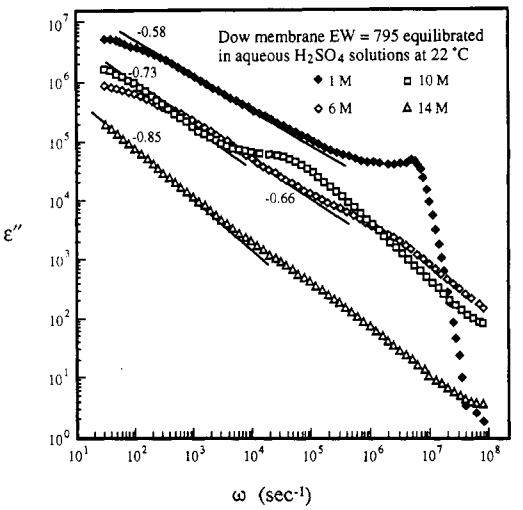

Figure 7. Dielectric relaxation loss curves for 795 EW membranes equilibrated in aqueous H_2SO_4 solutions of indicated molarities at 22 °C. The slopes of the low-frequency linear segments are listed.

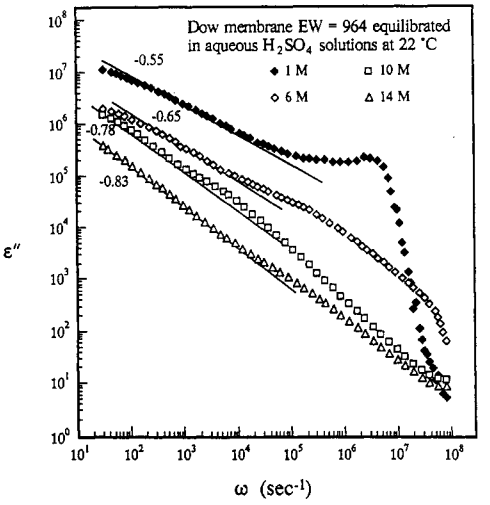

Figure 8. Same as in Figure 7 but for EW = 964.

per unit volume. The dipole in this case is the fluctuating cluster macrodipole referred to earlier. Long-range ion transport, of course, also contributes to dielectric permittivities but manifests its present mostly in the loss spectrum. In short, we believe that the extremely high observed values of ϵ_0 are, in effect, a signature of hydrophilic/hydrophobic microphase separation. The monotonic decrease in ϵ' with increasing frequency is due to the fact that the mobile ions become increasingly less able to follow the applied electric field reversals. This general behavior, of course, is typical of all dielectrics regardless of the relaxation mechanism.

Feature 3 is also present in loss spectra obtained in our similar studies of the long-side-chain PFSI membranes. As before, the linear log–log response is associated with long-range ion transport.

We will now discuss spectral aspects that are specific to the short-side-chain PFSI polymers.

Figures 7–9 show the loss spectra of membranes of 795, 964, and 1001 EW, respectively, having been equilibrated in H_2SO_4 solutions of 1, 6, 10, and 14 M concentrations at 22 °C. In addition to the general spectral features described above, the following finer details are noted. The log ϵ'' vs log ω plots were progressively depressed for all three equivalent weights as the H_2SO_4 concentration was increased. In addition, the relaxation peaks in the high-

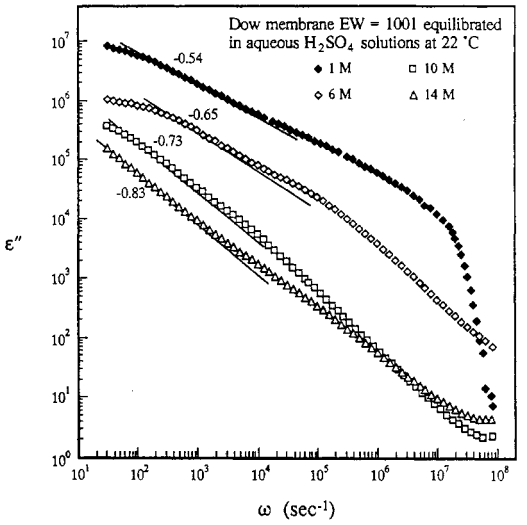

Figure 9. Same as in Figure 7 but for EW = 1001.

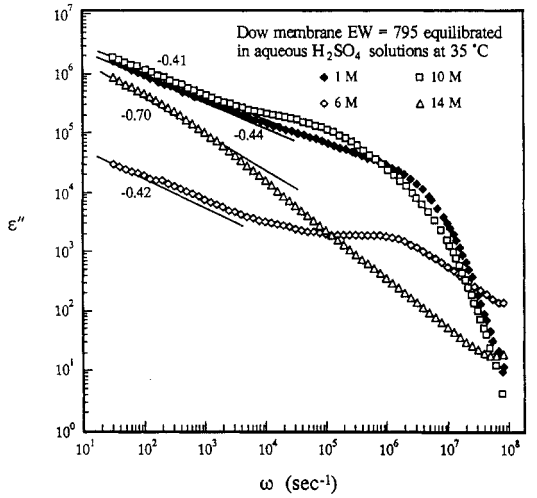

Figure 10. Dielectric relaxation loss curves for 795 EW membranes equilibrated in aqueous H_2SO_4 solutions of indicated molarities at 35 °C. The slopes of the low-frequency linear segments are listed.

frequency region became suppressed as the solution concentration increased. We believe that both of these trends are due to the fact that, as the clusters became less hydrated or as the cluster ionic microsolutions become more concentrated, ionic associations are forming. Continuing dehydration of the clusters would result in the gradual formation of a greater relative population of, first, partially-neutralized sulfate anions ($SO_4^{2-}H^+$), then electrically-neutral ion triplets ($H^+SO_4^{2-}H^+$), and then perhaps higher-order, rather sluggish multipoles at the highest concentrations, which would lead to an overall decrease of ionic mobility within the clusters. In one case, the magnitude of charge polarization that can develop at the hydrophilic/hydrophobic interfaces will diminish. Through the same ion-association agency, fewer ions will participate in long-range, i.e., *inter*cluster, transport because of their reduced mobility. Consequently, the entire loss spectra, including the relaxation peak, should be depressed with increasing acid concentration.

As seen in Figures 10–12, which refer to the same EW and acid concentration series as before but at the higher temperature of 35 °C, only the 1001 EW membrane completely exhibited the above-mentioned trends in the across-the-spectrum log ϵ'' vs log ω curve depression as well as the deteriorating relaxation peak definition with increasing H_2SO_4 concentration. While the 964 EW

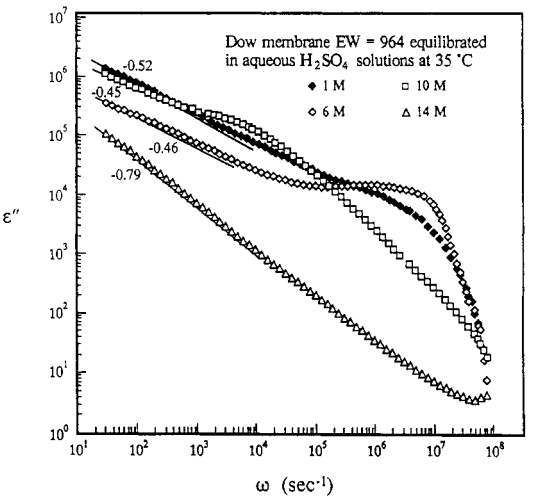

Figure 11. Same as in Figure 10 but for EW = 964.

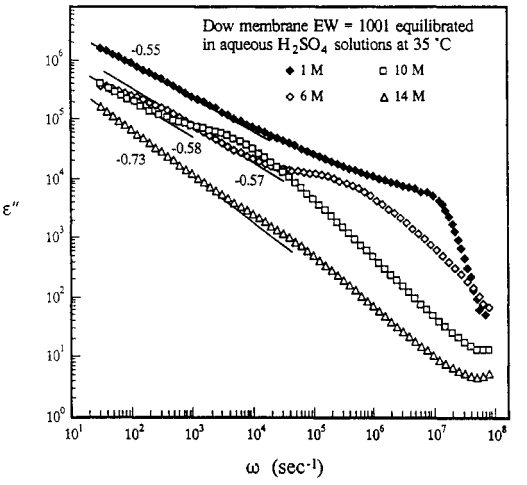

Figure 12. Same as in Figure 10 but for EW = 1001.

membrane maintains a semblence of these trends, with obvious deviations, the 795 EW membrane unquestionably breaks the pattern. Note that this pattern disruption increases with decreasing EW. As the ion-exchange capacity increases and the degree of crystallinity decreases with decreasing EW, one might expect the net electrolyte uptake to correspondingly increase. The electrolyte uptake will also increase, at a given EW, with increasing temperature. Perhaps the electrolyte uptake, as split between unequal concentrations of H^+ and SO_4^{2-} ions and water molecules, is a significant variable in generating this pattern-breaking behavior at 35 °C.

At 50 °C, the loss curves at all EW's lack the above-mentioned trend with acid concentration altogether and the curves are not vertically separated in the linear low-frequency regime to a high degree, as seen in Figures 13–15. However, the high-frequency relaxation always appears weakest at the highest concentration, as before. For this, as well as for the previous temperatures, this relaxation peak generally appears to shift to lower frequencies with increasing acid concentration. We rationalize this behavior in terms of a decreasing intracluster ionic mobility that is caused by a progressively greater degree of ionic association within the clusters. This mechanism would serve to increase the relaxation time for the dynamic interfacial polarization process.

At 65 °C, the loss curves, save for the 1001 EW case, have a greater concentration-induced vertical separation, at low frequencies, than that existing at 50 °C, as seen in Figures 16–18. At 795 EW, the vertical curve displacement

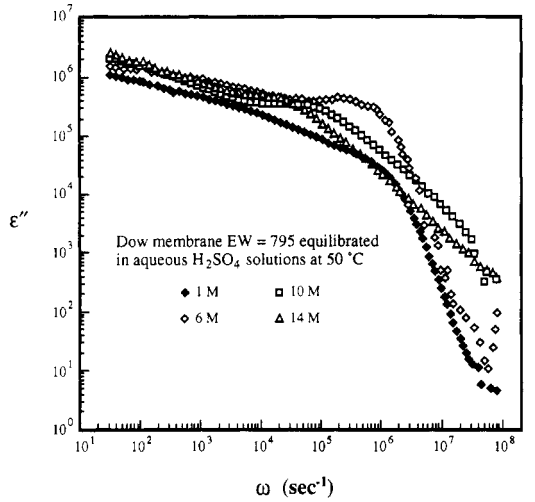

Figure 13. Dielectric relaxation loss curves for 795 EW membranes equilibrated in aqueous H_2SO_4 solutions of indicated molarities at 50 °C.

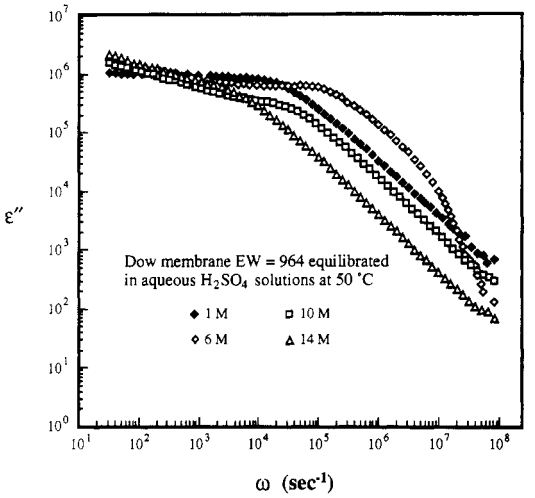

Figure 14. Same as in Figure 13 but for EW = 964.

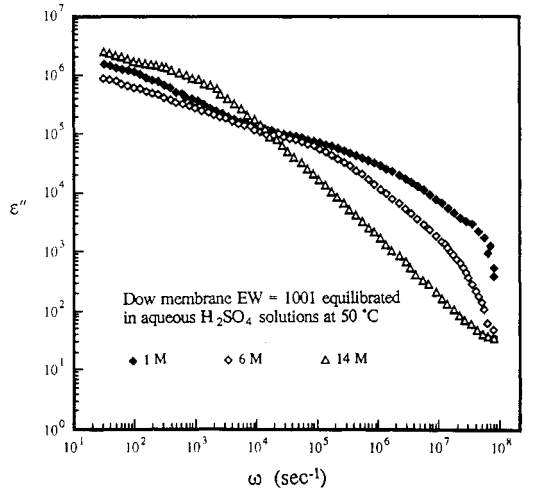

Figure 15. Same as in Figure 13 but for EW = 1001.

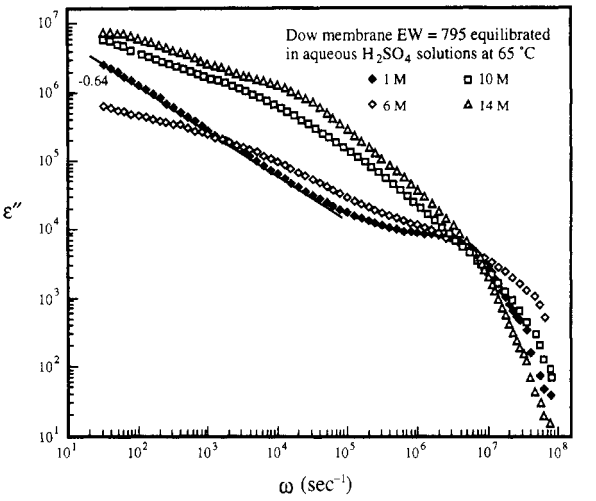

Figure 16. Dielectric relaxation loss curves for 795 EW membranes equilibrated in aqueous H_2SO_4 solutions of indicated molarities at 65 °C.

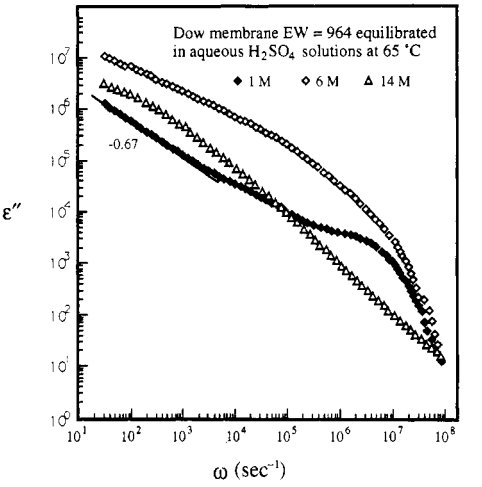

Figure 17. Same as in Figure 16 but for EW = 964.

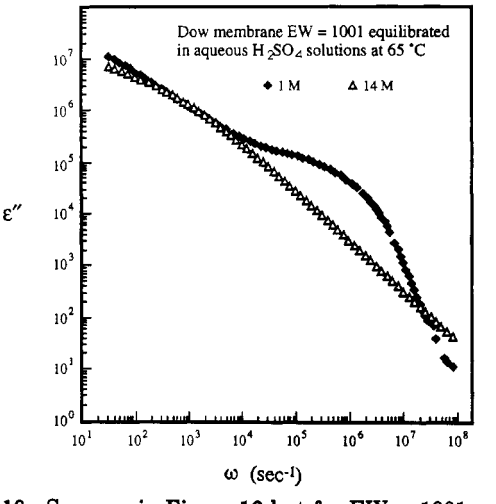

Figure 18. Same as in Figure 16 but for EW = 1001.

with increasing concentration is in fact somewhat upward, although two of the curves have a crossover point. Perhaps at this higher temperature and for this lowest EW membrane, which would be expected to contain the greatest concentration of water, the mobility-restricting association of ions has been reduced to a degree where the increase in ionic concentration from 1 to 14 M mainly affects an increase in the effective change carrier density within the membrane. Recall that electrical conductance can be generally represented as the product of the charge carrier density and the charge mobility. The increase in the number density of mobile ions in this way would, in effect, raise the log ϵ'' vs log ω curves as described by the ion-transport theory presented earlier, wherein the parameter K_1 is enhanced. Meaningful comment on the concentration dependence for the curves for 964 and 1001 EW is not possible as the data set is less complete. On the

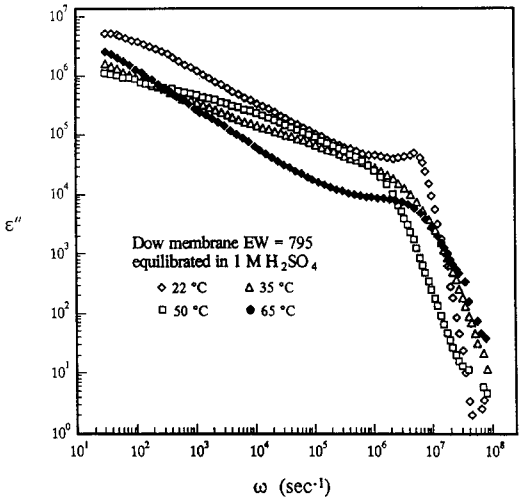

Figure 19. Dielectric relaxation loss curves for 795 EW membranes equilibrated in 1 M H_2SO_4 solutions at the indicated molarities.

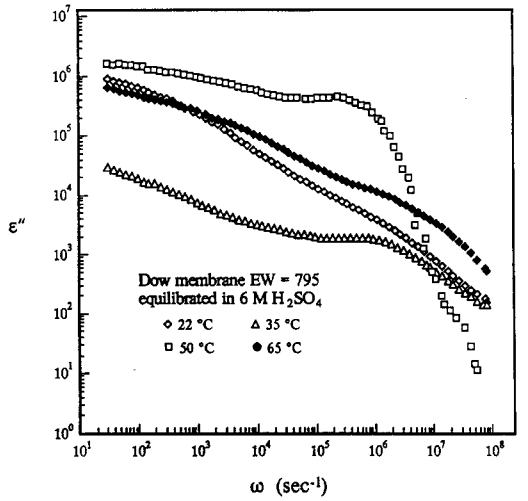

Figure 20. Same as in Figure 19 but for 6 M acid solutions.

other hand, at all three EW's, the relaxation peak does become less distinctive with increasing H_2SO_4 concentration, as before.

It would seem quite logical within the molecular-interpretive framework we have adopted for the observed dielectric relaxation behavior of these systems that, for a given EW and acid concentration, ϵ'' should increase across the spectra with increasing temperature. First, the volume fraction of the hydrophilic phase increases due to increased electrolyte sorption, and, second, the ionic mobility should be enhanced with increasing temperature. Figures 19–22 display loss spectra at the various indicated temperatures for the noted acid concentrations for EW = 795. At 1 and 6 M a monotonic ordering of the vertical displacement of the low-frequency loss curve segments, with temperature variance, is not present. On the other hand, the curves for 10 and 14 M are well-ordered, being monotonically displaced upward with increasing temperature in both cases. For the two highest concentrations, then, we suggest that an increasing ionic thermal kinetic energy progressively disrupts their bound associations so that the long-range contribution to ϵ'' is enhanced. Presently, however, we can offer no explanation for the confused behavior at the two lowest concentrations.

Figures 23–25 show the parameter n vs external H_2SO_4 concentration at the four temperatures and the three EW's. n at 22 °C is observed to increase in a rather linear fashion

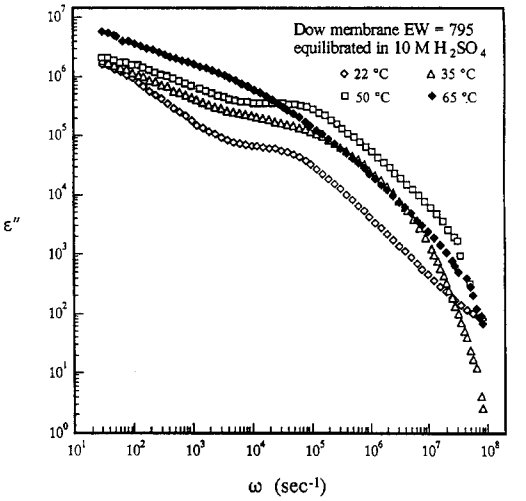

Figure 21. Same as in Figure 19 but for 10 M acid solutions.

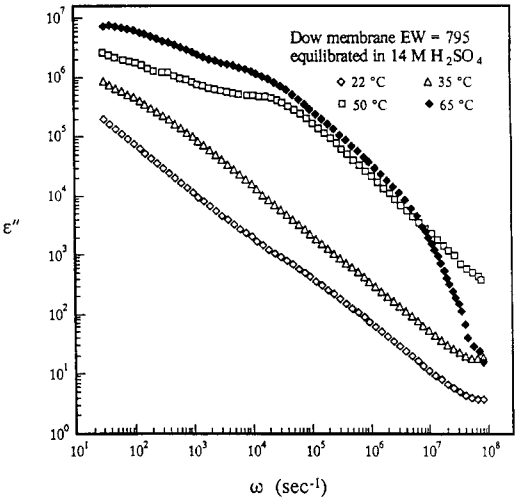

Figure 22. Same as in Figure 19 but for 14 M acid solutions.

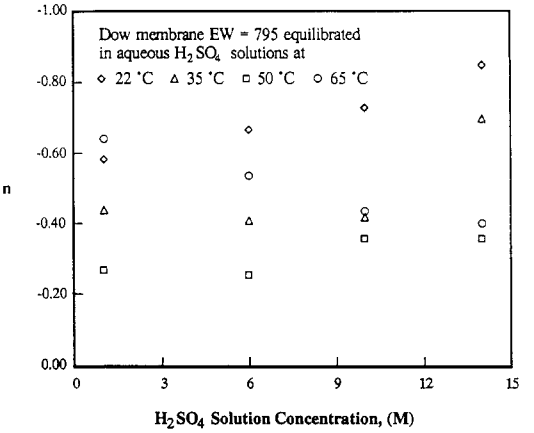

Figure 23. n vs H_2SO_4 concentration for the indicated temperatures for 795 EW membranes.

with increasing concentration for all three EW's. n starts from values depicting a transport situation that is a little less random than for pure diffusion at each EW. The highest n values, however, are not very close to that corresponding to pure ion migration, or drift. This trend is interpreted as being reflective of an increasingly greater connectivity of long-range ion-conductive pathways. One might imagine that, as the clusters deswell upon exposure to higher acid concentrations, they might pack more closely and thereby reduce activation energetic barriers for intercluster hopping. At 35 °C, n for all three EW's stayed

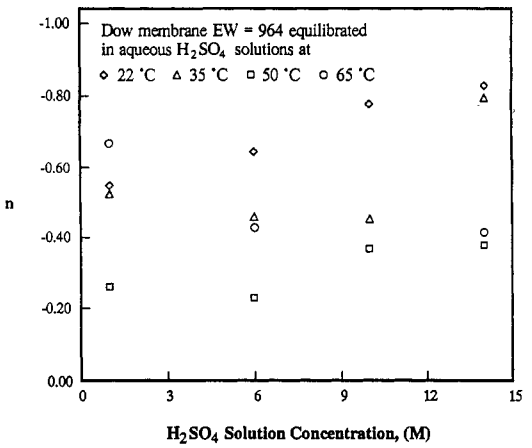

Figure 24. Same as in Figure 23 but for 964 EW membranes.

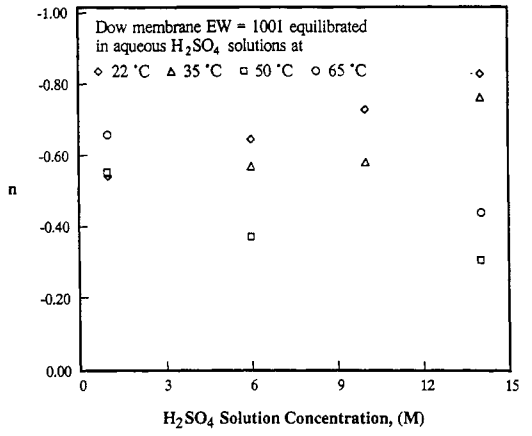

Figure 25. Same as in Figure 23 but for 1001 EW membranes.

somewhat constant at values corresponding to a condition of diffusion from 1 to 10 M and then abruptly increased from 10 to 14 M to a hybrid drift–diffusion condition. The 50 °C data are the most interesting in that the n values, while gradually increasing for the 795 and 964 EW membranes, remain in a "subdiffusion" state over the acid concentration range. Physically, these low n values would correspond to ion-hopping pathways that are more tortuous than those of random walks. One might perhaps think of a large number of ion traps, or dead ends, as existing on the overall ion-conduction grid in this case. A decrease in n with increasing concentration is actually seen for the 1001 EW membrane at 50 °C, which indicates increasing conduction pathway tortuosity. The graphs for 50 °C in fact contain the lowest n values at any acid concentration at any EW. Overall, the graphs shift downward with the two increases in temperature from 22 to 50 °C for all EW's. However, at 65 °C the downward graphical shifting trend is broken. Furthermore, n decreases with increasing acid concentration for all EW's at this temperature, although the absence of well-defined values of n in some instances prevented us from obtaining a complete data set. The values that were obtained for 65 °C are observed to lie in a range that reflects the dominance of diffusion over drift, and the diffusive pathways become more tortuous with increasing acid concentration.

ϵ_{ac}'' vs log ω curves were resolved from the ϵ'' spectra as described earlier. The resulting curves for membranes of 795 EW, for the four H_2SO_4 concentrations at 22 °C, are shown in Figure 26. First, it should be noted that these curve-resolved peaks are remarkably well-defined. There are basically two important observations to be made concerning these curves. The peak maxima shift to lower

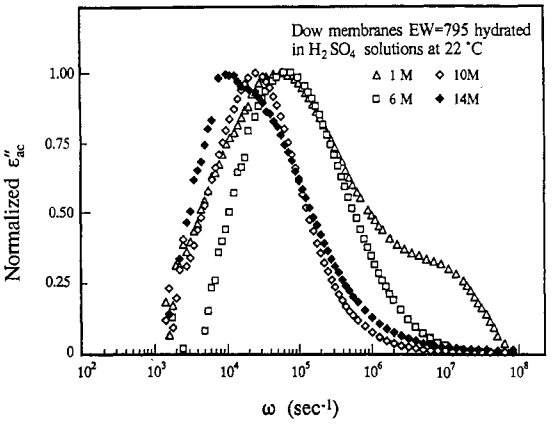

Figure 26. ϵ_{ac}'' vs log ω for 795 EW membranes equilibrated in aqueous H_2SO_4 solutions of indicated molarities at 22 °C. The peak heights have been rescaled so as to have the same value to permit better observation of peak frequency shifts.

frequencies with increasing H_2SO_4 concentration. This means that the time scale (τ) at which this relaxation is occurring is accordingly increasing. τ increases from somewhat greater than 10^{-5} to about 10^{-4} s from 1 to 14 M. In our previously-mentioned studies of numerous, similar aqueous electrolyte-containing, long- and short-side-chain perfluorosulfonate membranes, we attributed similar peaks in this region of loss spectra to the mechanism of relaxation of interfacial (hydrophilic/hydrophobic) polarization (Figure 2). In Figure 2, μ is an induced dipole moment for the cluster, α is an effective cluster polarizability, and δ is a phase angle that arises from the time lag of μ behind the applied oscillating field **E**. δ is due to the molecular impediments to ionic migration within the cluster. Throughout this rather simplistic discussion of *intra*cluster ion motions, it should be appreciated that the polarization fluctuations of a given cluster are most likely to be *coupled* to those of the other, at least nearest-neighbor, clusters.

Given this mechanistic assignment for the relaxation peak, we suggest that intracluster ionic motions become increasingly retarded with increasing H_2SO_4 concentration because of a progressively greater degree of ionic association. These molecular events would account for the corresponding increase in τ.

There also appears to be a narrowing of the peak widths with increasing concentration. As this implies a narrowing of the distribution of relaxation times and given the above mechanistic assignment, it is concluded that microstructural heterogeneity on the scale of cluster sizes becomes increasingly less severe with increasing acid concentration. Perhaps, with increasingly less water available to distribute throughout the membrane with increasing concentration, the distribution of ionic-hydration microstructures contained within the clusters must necessarily evolve to reflect a more homogeneous cluster environment. In this regard, we are referring to a combination of the size, shape, and chemical composition of a cluster and to the distribution of each of these factors in a rather general way.

It is very interesting to see, at the lowest concentration (1 M), an unmistakable shoulder superimposed on the high-frequency side of the peak. We interpret this *bimodal* relaxation behavior as arising from the coexistence of two distinct types of clusters at this lowest concentration. Perhaps the more liberal availability of incorporated water at 1 M allows for the formation of two different cluster-contained ionic-hydration microstructures. In this view, the high-frequency component might be associated with clusters having a comparatively larger ratio of water

Table I
High- and Low-Frequency Parameters of the Dielectric Relaxation Loss Spectra for Three Equivalent Weights as a Function of Acid Concentration at 22 °C

H_2SO_4 concn, M	EW = 795		EW = 964		EW = 1001	
	$(\omega_{ac})_{max}$	n	$(\omega_{ac})_{max}$	n	$(\omega_{ac})_{max}$	n
1.0	6.0×10^4	0.58	1.1×10^5	0.55	3.0×10^4	0.54
6.0	7.0×10^4	0.66	6.0×10^4	0.65	3.5×10^4	0.65
10	3.0×10^4	0.73	2.0×10^4	0.78	6.0×10^4	0.73
14	1.2×10^4	0.85	2.2×10^4	0.83	8.0×10^3	0.83

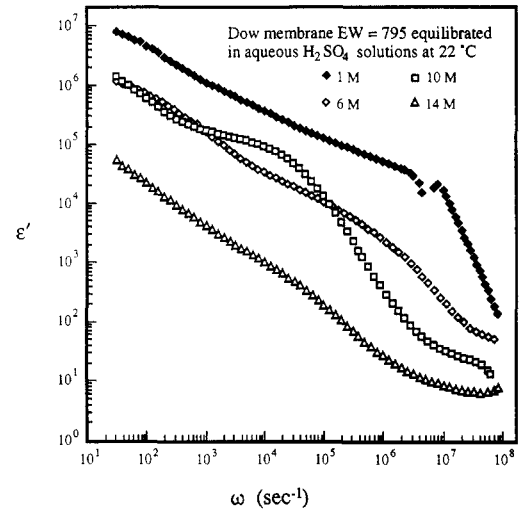

Figure 27. Dielectric relaxation storage curves for 795 EW membranes equilibrated in aqueous H_2SO_4 solutions of indicated molarities at 22 °C.

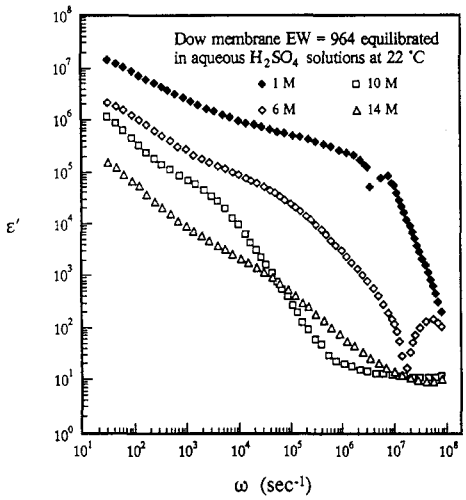

Figure 28. Same as in Figure 27 but for 964 EW membranes.

molecules to H_3^+O and SO_4^{2-} ions, which, in turn, would serve to impart a greater intracluster ionic mobility that accounts for the shorter relaxation time (10^{-7} s) displayed by this component.

The $(\omega_{ac})_{max}$ vs acid concentration behavior for the 964 and 1001, as well as for the 795 EW membranes, is seen in Table I. A general peak shift to low frequencies with increasing concentration, however, is not present, and no ordering of this quantity is apparent in this limited data set. The peak positions were all within the frequency range of 10^3–10^5 s^{-1}.

Shown in Figures 27–29 are the corresponding dielectric storage spectra for the 795, 964, and 1001 EW membranes. As before, the very high zero-frequency limit of this quantity, ϵ_0, is taken as a signature of microphase separation. The ϵ' vs f curves are steadily depressed with increasing acid concentration for all three equivalent

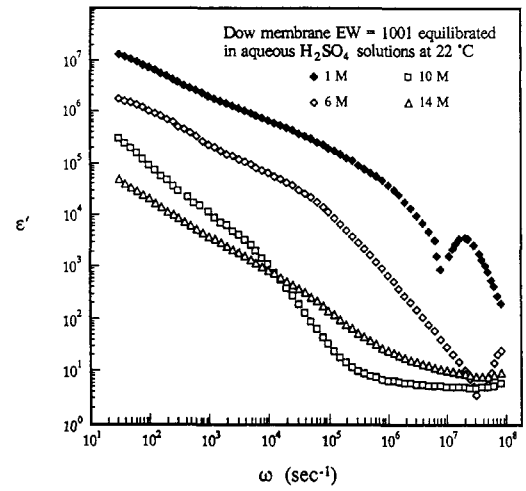

Figure 29. Same as in Figure 27 but for 1001 EW membranes.

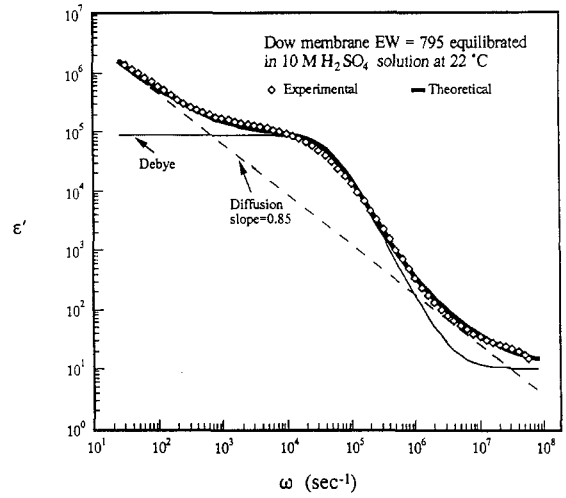

Figure 30. Experimental dielectric relaxation storage spectrum of a 795 EW membrane equilibrated in a 10 M H_2SO_4 solution at 22 °C. Also illustrated are the fitted theoretical ϵ' curve, based on the equivalent circuit model in Figure 4a, and the Debye-like and "diffusion" components of theoretical ϵ' for this model, vs ω.

weights at this temperature. We attribute this behavior, as in our earlier studies of aqueous NaOH-containing Nafion perfluorosulfonate membranes,[14] to a progressive decrease in ionic mobility with increasing concentration within the cluster microsolutions. In the general concept, ionic association inhibits interfacial polarization at all frequencies, resulting in a diminished induced cluster dipole moment. The dips seen in some of the storage curves at high frequencies correspond to the relaxation peaks in the loss spectra.

As in the case of the loss spectra, the storage spectra can also be mathematically resolved into basically two mechanistically-distinct components using eq 5, which applies to the equivalent circuit model in Figure 4a. Again, the two resolved components consist of (1) a reverse S-shaped Debye-like relaxation representing intracluster ion motions and the resultant cluster polarization and (2) a straight line with a theoretical, diffusion-related slope of $-1/2$ when $\log \epsilon'$ is plotted against $\log \omega$. In practice, the slope of the "diffusion" line is treated as a curve-fitted parameter. When the real part of eq 5 is fitted to the actual experimental curves, excellent fits are obtained, as seen in the examples in Figures 30 and 31. The cluster relaxation times extracted from these storage curve fittings are in fact quite consistent with those corresponding to the ϵ_{ac}'' vs ω peak positions, i.e., ω_{max}^{-1}. This manifestation

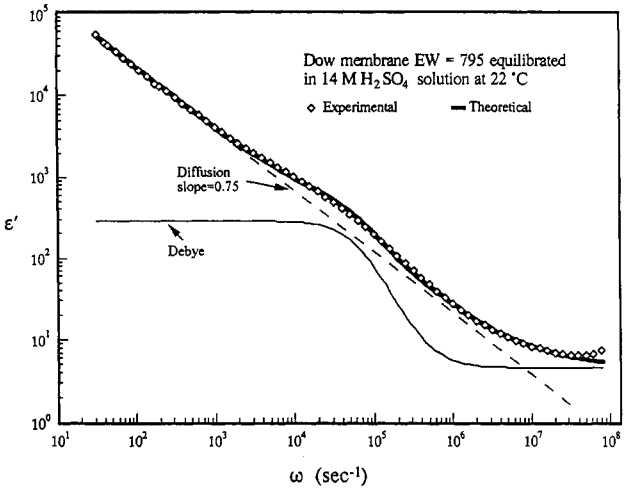

Figure 31. Same as in Figure 30 but for 14 M.

of self-consistency within the model is reassuring. On the other hand, the best-fitted slope of the line was −0.85 in Figure 30 and −0.75 in Figure 31, each of which is greater than the hypothetical slope of −0.5 for pure diffusion. Evidently, the long-range contribution to ϵ' involves ion migration that is more directed than that which occurs during pure diffusion. As in our earlier-discussed interpretation of the power law behavior of ϵ'' vs ω at low frequencies, a fractal concept might be appropriate wherein deviations of the exponent from $^1/_2$ are quite appropriate. Within this general interpretation, then, the equivalent circuit representation in Figure 4a seems to provide a very useful transport model, at least as a first approximation, wherein the various electrical impedance components have a distinct mechanistic interpretation within the framework of electrolyte-containing ionomers possessing a clustered morphology.

General Conclusions

We have performed a detailed, molecular-based dielectric relaxation analysis of aqueous H_2SO_4-containing Dow short-side-chain PFSI membranes. The following "fingerprints" of ion-transport and ionomer microstructure were identified in the relaxation spectra. The mechanistic-structural interpretations are largely based on our prior analyses of similar PFSI systems.

(1) Extremely high dielectric storage factors (ϵ'), especially at low frequencies, that imply a hydrophilic/hydrophobic microphase separation are universally observed. This morphological-based mechanistic assignment is, of course, in harmony with the known microstructure of these ionomeric systems.

(2) The occurrence of distinct linear segments in the low-frequency regime of all the log ϵ'' vs log ω plots is a clear signature of long range, i.e., *inter*cluster, ion transport. The slopes of these lines ($-n$) have been rationalized to be a coarse measure of the degree to which long-range ion displacements are controlled by ionic drift, diffusion, drift–diffusion hybrid situations, or transport that is in fact more tortuous than that corresponding to pure diffusion. It is suggested that the ion-conductive grid can be best described as being fractal in nature. In terms of polymer morphology, n is a crude measure of the degree of the ionic-hopping connectivity of the macroscopic ensemble of clusters such that the migration pathways become more tortuous with decreasing n. In many, but not all, cases of the H_2SO_4-containing membranes, it appears that long-range ion transport shifts from essentially diffusion toward drift control as the acid concentration increases. We envision that the decrease in membrane hydration attending an increase in acid concentration might shorten intercluster spacings overall and therefore drive n to the observed higher values. On the other hand, the depression of n with increasing temperature at all concentrations for all EW's might be a consequence of imparting a greater degree of random (i.e., as opposed to unidirectional), thermally-induced long-range ion motions. We regard this last suggestion, relating to the temperature dependence, as highly speculative.

Our basic proposition is that membranes displaying low n values have long-range ion-conductive pathways that are not highly interconnected and contain dead ends, i.e., charge traps. One might conjecture that methods of membrane synthesis or processing, or subsequent chemical or physical modifications that result in a more homogeneous microstructure (i.e., procedures that lead to systems with high n values), would be beneficial. It is well-known, for example, that annealing often serves to perfect polymer microstructures by inducing additional crystallinity in semicrystalline polymers or by affecting a reduction of free volume through more efficient chain packing in glassy polymers. A chemical factor that would seem to promote a homogeneous ionomer microstructure would be a narrow distribution of the number of CF_2 spacer units between the polar side chains, that is, a distribution of "local" equivalent weight. For a narrow EW distribution, the polymer chains could pack alongside each other with greater efficiency, forming better-developed TFE crystallites, and perhaps the side chains would be allowed to pack into clusters with greater efficiency than they would in the case of a considerable distribution in inter-side-chain CF_2 spacer lengths.

(3) In a number of cases, the vertical shifting of ϵ' and ϵ'' vs ω curves, either as a function of concentration at constant temperature or as a function of temperature at constant concentration, is rationalized in terms of electrostatically-bound associations of ions within cluster microsolutions.

(4) Relaxation maxima appearing in the high-frequency regime of the loss spectra were resolved from the curves by subtracting the long-range component, which is proportional to ω^{-n}, from ϵ'' in the high-frequency region. This relaxation is believed to be of an intracluster nature and to arise from the alternate accumulation and dissipation of net ionic charge at the hydrophilic/hydrophobic phase boundaries during a half-cycle of applied electric field oscillation. In short, the relaxation times derived from the peak positions are thought to represent the natural time scales during which these intracluster ionic displacements occur. It might in fact be true that the restraints on these short-ranged ion motions, e.g., cluster size, side-chain packing mode within clusters, and ionic-hydration structuring within the cluster microsolutions, especially at high acid concentrations, might constitute a rate-influencing factor in overall steady-state ion transport. The frequency shifts of the loss peak maxima with acid concentration, although showing trends in some instances, do not exhibit a universal behavior for all EW's and do not correlate as well as the parameter n does with concentration. An observed bimodal relaxation curve at the lowest concentration (highest water content) strongly suggests the coexistence of two distinct types of clusters in these membranes in this condition. The possibility of, and quantifying of, the distinction between different *types* of clusters in ionomers is an interesting morphological issue that would be difficult to explore with conventional

electron microscopic or small-angle X-ray scattering analyses.

Acknowledgment. Financial support received from Dow Chemical Co., as well as valuable technical discussions with C. W. Martin (Dow), is gratefully acknowledged.

References and Notes

(1) See examples of industrial applications in: Eisenberg, A., Yeager, H. L., Eds. *Perfluorinated Ionomer Membranes*; ACS Symposium *Series* 180; American Chemical Society: Washington, DC, 1982.
(2) Grot, W. G. *Chem.-Ing.-Tech.* **1978**, *50*, 299.
(3) Will, F. G. *J. Electrochem. Soc.* **1979**, *126*, 35.
(4) Yeo, R. S.; Chin, D.-T. *J. Electrochem. Soc.* **1980**, *127*, 546.
(5) La Conti, A. B.; Fragala, A. R.; Boyack, J. R. *Proc.-Electrochem. Soc.* **1977**, *77-6*, 354.
(6) Kakuta, N.; Park, K. H.; Finlayson, M. F.; Ueno, A.; Bard, A. J.; Campion, A.; Fox, M. A.; Webber, S. E.; White, J. M. *J. Phys. Chem.* **1985**, *89*, 732.
(7) (a) Olah, G. A.; Prakash, G. K. S.; Sommer, J. *Science* **1979**, *206*, 13. (b) Olah, G. A.; Meidar, D.; Mulhotray, R.; Narang, S. C. *J. Catal.* **1980**, *61*, 96. (c) Waller, F. J. In *Catalytic Conversions of Synthesis Gas and Alcohols to Chemicals*; Hermen, R. G., Ed.; Plenum: New York, 1984; p 193.
(8) Lowry, S. R.; Mauritz, K. A. *J. Am. Chem. Soc.* **1980**, *102*, 4665.
(9) Mauritz, K. A.; Gray, C. L. *Macromolecules* **1983**, *16*, 1279.
(10) Falk, M. In *Perfluorinated Ionomer Membranes*; ACS Symposium Series 180; American Chemical Society: Washington, DC, 1982; p 139.
(11) Yeo, S. C.; Eisenberg, A. *J. Appl. Polym. Sci.* **1977**, *21*, 875.
(12) Kyu, T.; Hashiyama, M.; Eisenberg, A. *Can. J. Chem.* **1983**, *61*, 680.
(13) Hodge, I. M.; Eisenberg, A. *Macromolecules* **1978**, *11*, 289.
(14) Mauritz, K. A.; Fu, R.-M. *Macromolecules* **1988**, *21*, 1324.
(15) Mauritz, K. A.; Yun, H. *Macromolecules* **1988**, *21*, 2738.
(16) Mauritz, K. A.; Yun, H. *Macromolecules* **1989**, *22*, 220.
(17) Mauritz, K. A. *Macromolecules* **1989**, *22*, 4483.
(18) Starkweather, H. W., Jr.; Chang, J. J. *Macromolecules* **1982**, *15*, 752.
(19) Boyle, N. G.; McBrierty, V. J.; Eisenberg, A. *Macromolecules* **1983**, *16*, 80.
(20) McBrierty, V. J.; Douglass, D. C. *Macromol. Rev.* **1981**, *16*, 295.
(21) Boyle, N. G.; McBrierty, V. J.; Douglass, D. C. *Macromolecules* **1983**, *16*, 75.
(22) Komoroski, R. A.; Mauritz, K. A. *J. Am. Chem. Soc.* **1978**, *100*, 7487.
(23) Komoroski, R. A.; Mauritz, K. A. Reference 10, p 113.
(24) Mauritz, K. A.; Rogers, C. E. *Macromolecules* **1985**, *18*, 483.
(25) Starkweather, H. W., Jr. *Macromolecules* **1982**, *15*, 320.
(26) Hashimoto, T.; Fujimura, M.; Kawai, H. Reference 10, p 217.
(27) Pineri, M.; Duplessix, R.; Volino, F. Reference 10, p 249.
(28) Gierke, T. D.; Munn, G. E.; Wilson, F. C. *J. Polym. Sci., Polym. Phys. Ed.* **1981**, *19*, 1687.
(29) Mauritz, K. A. *J. Macromol. Sci., Rev. Macromol. Chem. Phys.* **1988**, *C28* (1), 65.
(30) Ezzell, B. R.; Carl, W. P.; Mod, W. A. In *Industrial Membrane Processes*; AIChE Symposium Series 248; White, R. E., Pintauro, P. N., Eds.; American Institute of Chemical Engineers: New York, NY, 1986; p 45
(31) Tant, M. R.; Darst, K. P.; Lee, K. D.; Martin, C. W. In *Multiphase Polymers: Blends and Ionomers*; ACS Symposium Series 395; Utracki, L. A., Weiss, R. A., Eds.; American Chemical Society: Washington, DC, 1989, p 370.
(32) Moore, R. B.; Martin, C. R. *Macromolecules* **1989**, *22*, 3594.
(33) Donnan, F. G. *Z. Elektrochem.* **1911**, *17*, 572; *Chem. Rev.* **1924**, *1*, 73.
(34) Mauritz, K. A., unpublished results.
(35) Gabrielli, C. Solartron Technical Report 004/83; Solartron Instruments, Farnsborough, UK, 1984; p 3.
(36) Raistrick, I. D.; Macdonald, J. R.; Franceschetti, D. R. In *Impedance Spectroscopy*; MacDonald, J. R., Ed.; John Wiley & Sons: New York, 1987, Chapter 2.